IGTC-2019-130

Proceedings of the International Gas Turbine Congress 2019 Tokyo
November 17-22, 2019, Tokyo, Japan

Identification of low speed fan flutter trigger through radial decomposition of the modeshape

Quentin Rendu[1], Sina Stapelfeldt[1], Loic Salles[1] and Mehdi Vahdati[1]

[1] Vibration University Technology Center
Mechanical Engineering Department
Imperial College London
London SW7 2AZ, UK

ABSTRACT

Assessing the aeroelastic behavior of blades is a crucial step in modern jet engines design. In recent years, efforts have been done to build whole assembly models of fan flutter. Flutter results from a competition of complex phenomena such as shock-wave oscillation, boundary-layer separation and acoustic reflections. To identify the mechanism triggering the instability, a radial decomposition strategy based on a linear superposition principle is applied to a transonic fan. The geometry consists of the low-pressure part of the engine, namely the air intake, the fan, the outlet guide vane and the engine section stators. Experimentally, flutter was encountered in the first bending mode at part speed. 3D URANS aeroelastic computations are able to reproduce the flutter instability. The modeshape is then radially split into ten independent panels. One aeroelastic computation is performed for each panel, giving the radial contribution to the global damping coefficient. The most destabilising contribution is found at 80% span, below the least stable radial level (90% span). These results indicate that some radial migration of the pressure fluctuations is responsible for stall flutter.

INTRODUCTION

Aeroelasticity is one of the main concerns during the design of future jet engines. Due to large diameter and light materials, flutter may be experienced by fan blades. Computational Fluid Dynamics (CFD) is used to predict fan flutter boundary in the early design steps. In recent years, efforts have been made to build 3D models of fan flutter. These models are accurate enough to describe the flutter boundary of an engine fan, eventually taking into account acoustic wave reflections at the intake. These computations show that the exchange of energy between the fluid and the structure is mainly done between 80% and 90% of the blade height [1, 2]. Thus, the damping coefficient of the blade is sometimes approximated by 2D computations near the blade tip.

During stall flutter, the blades vibration generate shock-wave oscillations, fluctuations of the boundary layer and propagation of acoustic waves in three directions. The interactions of all these unsteady mechanisms leads to aerodynamic forces whose resultant is destabilising. Because of these interactions, the identification of flutter sources is a real challenge. Detailed analysis of the unsteady flow provides insights but may not be sufficient. To overcome this challenge, one can decompose the response of the flow into a sum of responses to elementary perturbations. Such a decomposition relies on the linearity of the flow with respect to time. This approach has been used by Ferrand [3] to analyse choke flutter contributions using a coupled 1D/2D linearised Euler method. It has been extended to two dimensional turbulent flow using a linearised RANS solver [4]. Recently, it has been applied for the first time using a 3D nonlinear time-marching RANS solver [5]. The computational domain used was a single passage fan blade row and the results showed that radial migration of pressure fluctuations trigger stall flutter. The present work aims at extending the method to full-annulus computation of the whole low pressure compressor of the engine, namely fan, outlet guide vane (OGV) and engine section stators (ESS).

The numerical methods are presented in the next section. The decomposition method is then validated on full-annulus computations of stall flutter using a 3D nonlinear RANS solver. The method is finally used to identify the contribution of the different radial layers to the aeroelastic instability.

COMPUTATIONAL METHODS

The Unsteady Reynolds-Averaged Navier-Stokes (URANS) solver AU3D is used to perform all the computations. It has been developped at Imperial College with the support of Rolls-Roycs and has been extensively validated over the past 25 years. It relies on a

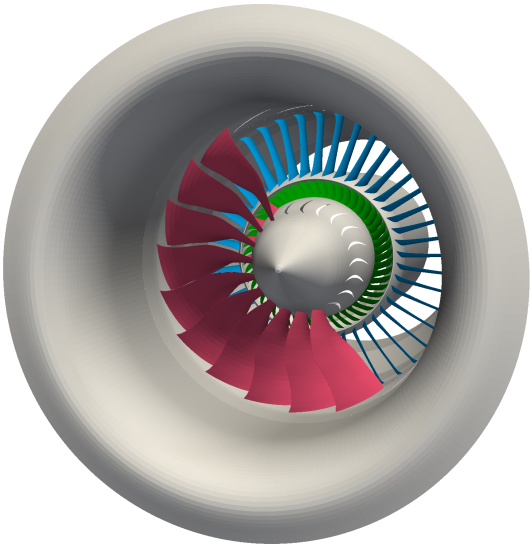

Fig.1 Front view of the computational domain including the nacelle (grey), the fan blades (red, only half of the fan is shown for clarity), the outlet guide vane (blue) and the engine section stators (green)

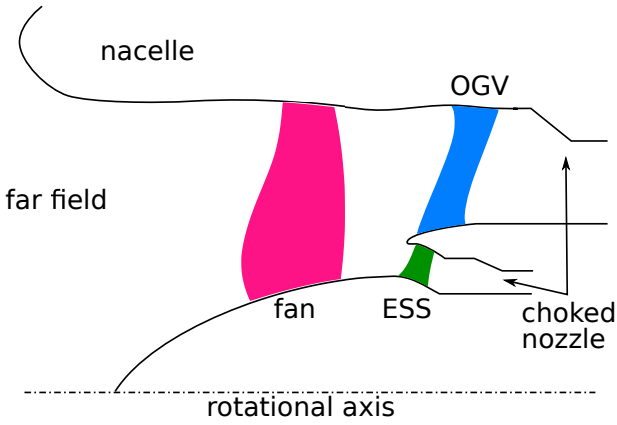

Fig.2 Sketch of the computational domain, fan blades are rotating while outlet guide vanes (OGV) and engine section stators (ESS) are stationary

time-domain finite volume method on a multi-block unstructured grid. The turbulence is modelled through Spalart-Allmaras model with wall functions [6]. More details can be found in [7].

The computational domain includes the intake, the low speed fan (20 blades), outlet guide vanes and engine section stators. A 3D view of all these components is shown in Fig. 1. The domain inlet is located 100 fan chords upstream of the engine intake. Sea level total pressure and total temperature, as well as zero flow angles are prescribed there as boundary conditions. Downstream of the stator blade rows, a choked nozzle is added, consisting of a converging duct and a very low static pressure at the outlet (see Fig. 2). This avoids numerical reflections of acoustic waves on the outlet boundary condition. To reduce the number of mesh points, the fan tip clearance is not modelled and all the endwalls are considered inviscid. All the blades (fan, OGV and ESS) are computed using Spalart-Allmaras turbulence model with wall functions [6]. The fan mesh contains 20 layers in the spanwise direction and around 250 points on the blade profile. Upstream of the fan, the mesh is fine enough to accurately compute the propagation and reflection of acoustic waves at the blade vibrational frequency and nodal diameter. The total size of the mesh is around 10 million points.

For steady computations, a single passage mesh is used with periodic boundary conditions and mixing plane between the rotating row (the fan blades) and the stationary ones (intake, OGV, ESS). For aeroelastic simulations, a full-annulus mesh is used with sliding planes between rotating and stationary rows. The vibration of each fan blade is imposed, based on the first flap modeshape and the nodal diameter. Time-marching is performed using dual time stepping procedure, consisting of a Newton-Raphson method with inner implicit step (Jacobi algortihm is used to solve the the linear system). The number of time-step per vibration cycle is set to 240. The computation starts with a transient regime before reaching a periodic solution. The aerodynamic forces are then extracted to compute the work extracted by the fluid to the structure, on each point of the blade surface. In this work, negative work and negative damping coefficient denote unstable aeroelastic response.

RESULTS

Flutter event

The Mach number of the blade tip is used to characterise the rotational speed:

$$M_{tip} = \omega r_{tip}/a \qquad (1)$$

A flutter zone has been measured experimentally at part speed ($0.86 < M_{tip} < 0.98$). The involved modeshape corresponds to

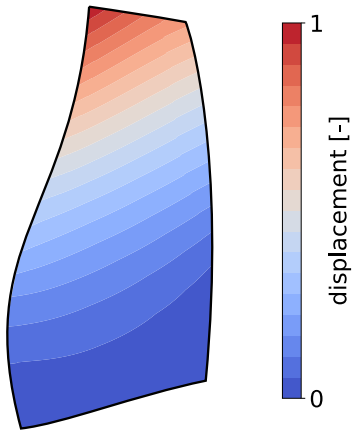

Fig.3 Normalised displacement for the first flap mode (1F)

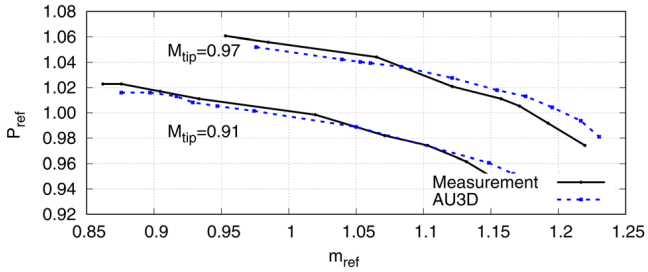

Fig.4 Comparison of AU3D and measured characteristics at $M_{tip} = 0.91$ and $M_{tip} = 0.97$ from [8]

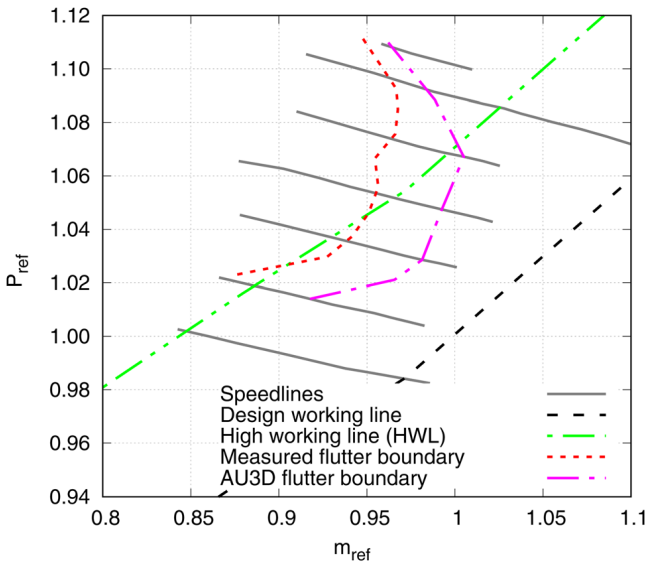

Fig.5 Fan map and flutter boundary from [8]

the first flap mode (1F) at nodal diameter 3ND. The normalised displacement associated with this modeshape is shown in Fig. 3. The corresponding reduced frequency, based on relative velocity and chord at 90% span, is 0.12. A previous paper [8] showed the ability of AU3D to reproduce the steady characteristic as well as the flutter boundary (see Fig. 4 and Fig. 5).

A steady computation is run at $M_{tip} = 0.93$, in the middle of the flutter region. The axial velocity and streamlines, at an operating

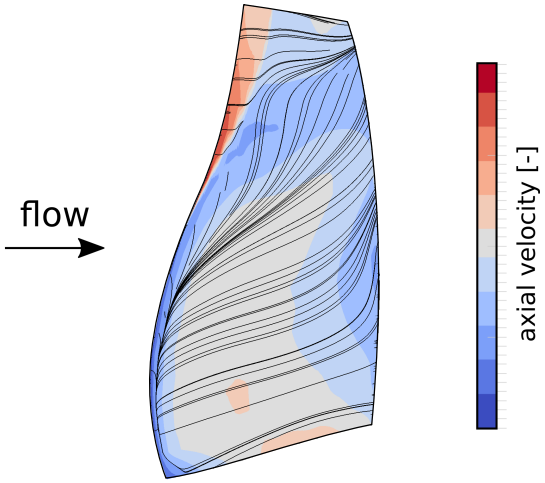

Fig.6 Steady streamlines and axial velocity on suction surface

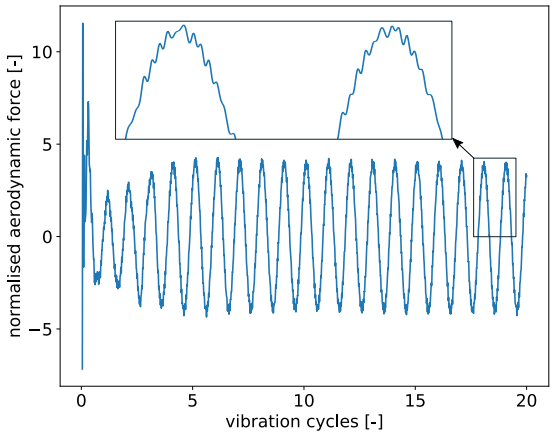

Fig.7 Normalised aerodynamic modal force along vibration cycle

point close to the surge line, are plotted on the suction surface in Fig. 6. The red zone close to the leading edge, from 60% span to tip, corresponds to the supersonic region. It is terminated by a strong shock-wave. A large radial migration of the flow can be observed through the streamlines. This separation is typical of stall flutter events [2].

To assess the aeroelastic response of the fan blades, the aerodynamic modal force is recorded during the computation. It is plotted along vibration cycles in Fig. 7. A strong transient regime is observed during the five first cycles, after which a periodic regime is obtained. A zoom on the signal shows higher harmonics which corresponds to rotor/stator interaction. The wakes of the fan blades impact the downstream stator rows, generating acoustic waves which are able to travel upstream and to impact fan blade pressure distribution. To quantify the contribution of these higher modes, the frequency spectrum is plotted in Fig. 8. The main peak, associated to the blade vibration, can clearly be seen at $f/f_{vib} = 1$. The second most energetic peak, observed at $f/f_{vib} = 25.6$, has an amplitude 25 times smaller than the main peak. This indicate that the flow response is quasilinear as it mainly responds at the vibrational frequency.

The aerodynamic damping coefficient associated to the periodic state is $\zeta = -0.0071$. It is negative, indicating a flutter instability.

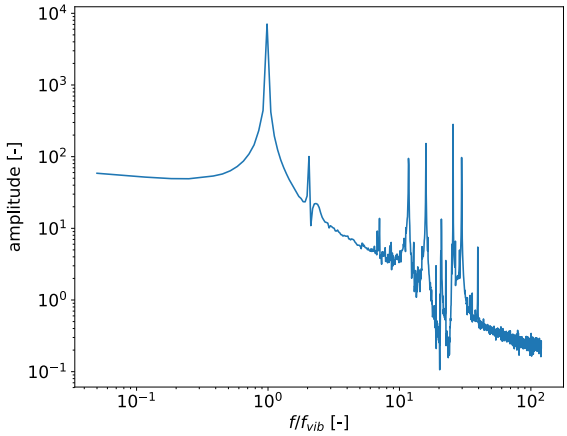

Fig.8 Spectrum of aerodynamic modal force amplitude based on the last 15 cycles (f_{vib} is vibrational frequency)

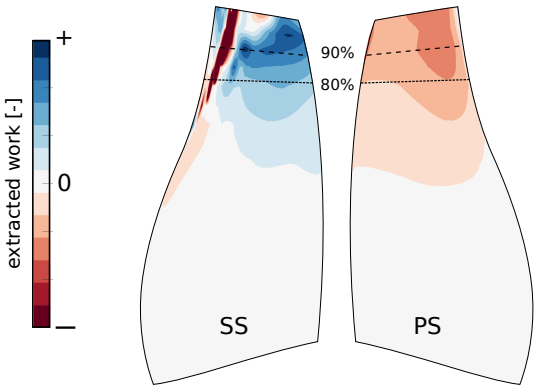

Fig.9 Normalised work extracted by the flow on blade suction surface (SS) and pressure surface (PS) for the full blade vibration - negative (red) depicts instability

To further investigate the aeroelastic behavior of the blade, the local aerodynamic work is plotted in Fig. 9. The exchange of energy is mainly done close to the tip of the blade, above 80% span. The pressure side is destabilising everywhere. The highest destabilising contribution is observed close to the tip and near the leading edge, where the blade's displacement is the highest (see Fig. 3). On the suction side, there is a competition between a strong destabilising contribution of the shock-wave, followed downstream by a stabilising contribution down to the trailing edge. These competing effects finally lead to an aeroelastic instability where the exchange of energy between fluid and structure seem to be mostly located above 90% span. For this rotational speed, the shock-wave contribution switches from stabilising at higher mass-flow (close to the design point) to destabilising during flutter.

Verification of decomposition methodology

As the blade vibrates, acoustic waves are generated on the blade surface, at the leading and trailing edge, in the vicinity of the shock-wave or in the wake. All these pressure waves propagate in the blade row, as well as upstream and downstream where the may be reflected. The previous analysis allows to identify where the pressure fluctuations interact the most strongly with the structure vibration, but it does not indicate where these pressure fluctuations come from. To address this issue, the blade modeshape is radially decomposed into ten panels as shown in Fig. 10. All the panels have the same number of points and include two radial

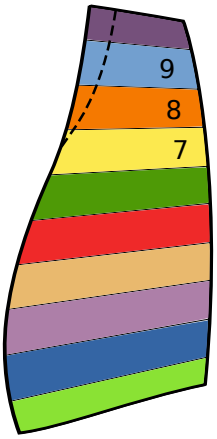

Fig.10 Radial decomposition of the modeshape in ten panels - dashed line denotes the steady position of the shock-wave

levels of the mesh. Ten unsteady computations are run, each of them with one panel vibrating. The 3D unsteady pressure is then projected on the full modeshape to compute the work extracted by the flow. The decomposition of the unsteady flow in the sum of unsteady flows relies on the linear superposition principle. To stay in the linear regime, a very small displacement is imposed, corresponding to 0.05% of the blade chord. Thanks to this small value, the discontinuity between two adjacent panels is very small and does not need to be smoothed. The computations start with a transient state and are run until a periodic state is reached. The results presented in this work are obtained using the 20th vibration cycle (modal response does not depend on the chosen cycle in the periodic state).

If the linear superposition is valid (*i.e.* the flow fluctuations are small enough) and the results converged (*i.e.* the flow reaches a periodic state), the sum of the damping coefficients obtained as each individual panel vibrates, must match the damping coefficient obtained as the full blade vibrates. To verify this, the work is plotted along span in Fig. 11. The agreement is excellent between the two methods. A small discrepancy is observed for the two radial points close to the tip. This is explained by numerical errors which prevent a pure periodic state. The accuracy of the decomposition methodology with respect to the global aerodynamic damping coefficient is 97.7%. It is thus accurate enough to use it to identify the source of the instability.

Principal aeroelastic contribution

The spanwise distribution of extracted work, plotted in Fig. 11, confirms that the energy is mainly exchanged near the tip of the blade. It also indicates that each radial level is globally unstable. It means that each stabilising contribution (the blue regions in Fig. 9) is counterblanaced by a stronger destabilising contribution at the same radial level.

To evaluate the contribution of each radial level to the global instability, the contribution of each panel is plotted in Fig. 12. A remarkable fact is that all panels have a destabilising contribution, which differs from a previous study at a similar rotational speed where only the fan blade row was modelled [5]. In this work, the vibration of the fan blades generates pressure waves which propagate upstream, are reflected at the air intake and then come back to the fan blade row. This mechanism is the main reason for the stall flutter region in the fan operating range [9]. The phase-shift

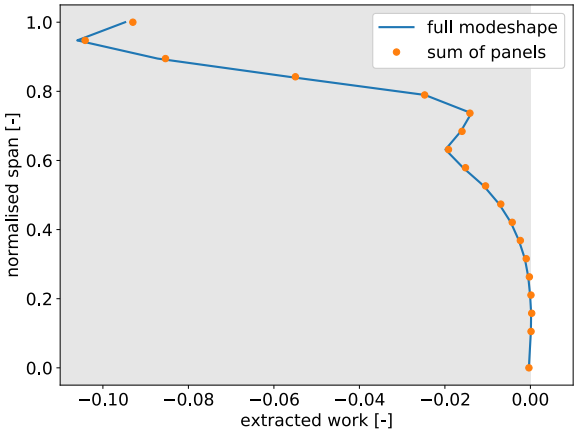

Fig.11 Work extracted by the flow along span for the full blade vibration (solid line) and the decomposition method (symbols)

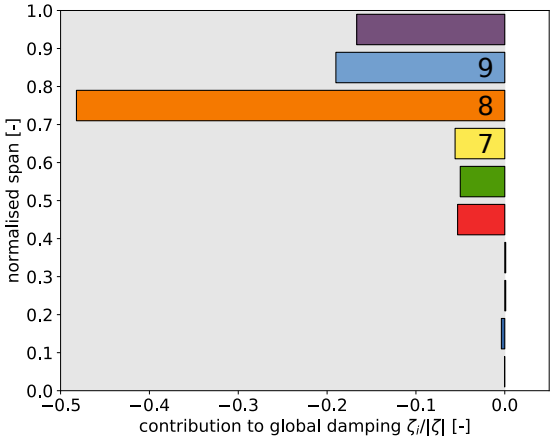

Fig.12 Contribution due to vibration of each panel to the global damping (see Fig. 10 for corresponding colors)

between the wave generated in the blade row and the reflected one when it reaches the fan again only depends on the steady flow and the length of the intake. This acoustic contribution would thus be destabilising for all the panels, and its amplitude would depend on the blade's displacement, which scales with radius.

Looking more closely, the graph shows that the contribution of the first four panels ($h < 40\%$) is negligible. Their contribution was expected to be small because the displacement of the blade is smaller near the hub. The fact that panels 3 and 4 have a lower contribution than panel 2 indicate that stabilising and destabilising regions cancel each other. Panels 5, 6 and 7 ($40\% < h < 70\%$) have a similar destabilising contribution of around 5%. Panel 8 ($70\% < h < 80\%$) is the most destabilising one, contributing for almost half of the total instability. Panels 9 and 10 ($80\% < h$) have a similar destabilising contribution of around 15%. This analysis finally shows that one panel is responsible for half of the total aerodynamic damping. In other words, it contributes as much as the other panels all together.

To further investigate the different contributions associated to panels 5 to 10, the extracted work is plotted in Fig. 13. Panels 5, 6 and 7, located between 40% and 70% span, show very low extracted work. The only significative regions are a small stabilising contribution on the suction side, close to the leading edge and at the

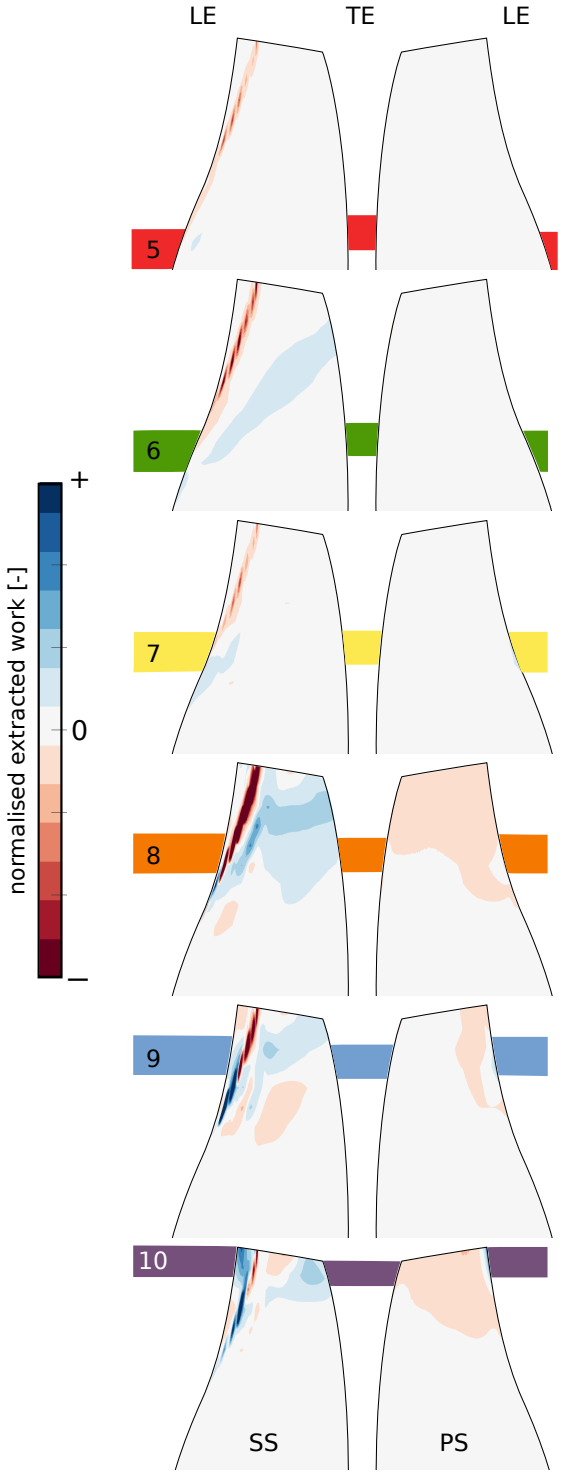

Fig.13 Normalised work extracted by the flow on blade suction surface (SS) and pressure surface (PS) for the vibration of panels 5 to 10 - background rectangles depict the position of the vibrating panel

radial level of the panel itself. Above of the panel, a destabilising contribution is seen at the steady position of the shock-wave. This indicates that pressure waves are locally stabilising while they have a destabilising effect on the shock-wave located above. The amplitude is very small because the steady position of the shock-wave does not reach panels 5 to 7 (see Fig. 10). Note that panel 6 exhibits slightly higher levels of extracted work. Because the blade vibration is smaller than for panel 7, it indicates that the pressure waves generated by panel 6 do not have a higher amplitude but a different phase shift when reaching the shock-wave.

The extracted work associated to panel 8 is very strong. One explanation could be that the panel is located at the lower radial extent of the shock-wave, where there is a sonic point (point at which the flow reaches a relative Mach number equal to 1). It has been shown by Ferrand [3] that pressure waves generated at a sonic point quickly grow in amplitude. These pressure waves can migrate radially and impact the shock-wave, which will start to oscillate strongly. The contribution of the shock-wave being everywhere destabilising, one can conclude that these pressure waves reach it with approximately the same phase-shift. On the suction side, a large stabilising region starts at the leading edge, close to the lower end of panel 8, and migrates downstream as well as radially. It finally spans most of the suction surface behind the shock-wave, and has a greater amplitude than the destabilising contribution on the pressure side. The quick rise of destabilising contribution between panel 7 and 8 (see Fig. 12) can thus be explained by an increase of the amplitude of pressure fluctuations due to the shock-wave oscillation.

Concerning panel 9, the amplitude of extracted work is still very high. The shock-wave is not completely destabilising anymore: a stable region appears below 80% span (hence below the panel itself). The amplitude of this contribution is large and counterbalances the destabilising effect of the shock-wave closer to the tip. The sharp drop of destabilising contribution between panel 8 and 9 (see Fig. 12) thus result from a new behavior where two regions compete, rather than a decrease of the pressure fluctuations amplitude. Panel 10 is very similar to panel 9, but with a stronger destabilising contribution of the pressure side and a weaker destabilising contribution of the shock-wave. The switch from a completely destabilising contribution of the shock-wave to a competition of two regions was also reported in [5]. This analysis confirms that radial migration is responsible for stall flutter and that the main destabilising contribution will be reached below the least stable level, around the radial position of the sonic point.

CONCLUSIONS

This work is a new step towards the understanding of fan stall flutter in modern jet engines. A decomposition methodology based on a linear superposition principle has been successfully applied. The results show that the radial level contributing the most to the instability is not the least stable level ($h > 90\%$), but is located below ($70\% < h < 80\%$). Moreover, a local stabilising contribution of the leading edge was observed, confirming a previous study.

Further analysis could help to decouple the influence of the air intake with the blade's behaviour itself. Another decomposition, based on the blade chord rather than its span, could also help to understand the contribution of the leading and trailing edge vibration, as well as the local excitation of the shock-wave. These new hindsights would prove useful to design active or passive control systems for fan flutter.

ACKNOWLEDGEMENTS

The authors thank Rolls-Royce plc for both sponsoring this work and allowing its publication.

References

[1] Aotsuka, M., and Murooka, T., 2014.
"Numerical analysis of fan transonic stall flutter".
In ASME Turbo Expo 2014: Turbine Technical Conference and Exposition, American Society of Mechanical Engineers, p. V07BT35A020.

[2] Vahdati, M., and Cumpsty, N., 2016.
"Aeroelastic instability in transonic fans".
journal of Engineering for Gas Turbines and Power, ***138***(2), p. 022604.

[3] Ferrand, P., 1984.
"Linearized theory of the choked flow in an annular oscillating cascade".
In Unsteady Aerodynamics and Aeroelasticity of Turbomachines and Propellers, 3rd International Symposium, Ed Cambridge University, pp. 41–52.

[4] Rendu, Q., Aubert, S., and Ferrand, P., 2017.
"Influence of reduced frequency on choke flutter in transonic UHBR fan".
In International Forum on Aeroelasticity and Structural Dynamics, pp. 1812–1826.

[5] Rendu, Q., Salles, L., and Vahdati, M., 2018.
"Radial decomposition of blade vibration to identify stall fluttersource in a transonic fan".
In 15th International Symposium on Unsteady Aerodynamics, Aeroacoustics & Aeroelasticity of Turbomachines.

[6] Spalart, P., and Allmaras, S., 1992.
"A one-equation turbulence model for aerodynamic flows".
In 30th Aerospace Sciences Meeting, p. 439.

[7] Sayma, A., Vahdati, M., and Imregun, M., 2000.
"An integrated nonlinear approach for turbomachinery forced response prediction. part i: Formulation".
Journal of fluids and structures, ***14***(1), pp. 87–101.

[8] Stapelfeldt, S., and Vahdati, M., 2018.
"On the importance of engine-representative models for fan flutter predictions".
Journal of Turbomachinery, ***140***(8), p. 081005.

[9] Zhao, F., Smith, N., and Vahdati, M., 2017.
"A simple model for identifying the flutter bite of fan blades".
Journal of Turbomachinery, ***139***(7), p. 071003.